Arch Appl Mech (2011) 81:1351–1363
DOI 10.1007/s00419-010-0487-7

ORIGINAL

S. Wang · H. Zhang

Partition of unity-based thermomechanical meshfree method for two-dimensional crack problems

Received: 12 March 2010 / Accepted: 11 November 2010 / Published online: 8 December 2010

Abstract We present a partition of unity-enriched element-free Galerkin method for thermoelastic two-dimensional crack problems. Therefore, the displacement field is enriched by the step enrichment. In the vicinity of the crack tip, the asymptotic branch enrichment functions commonly used in linear elastic fracture mechanics are employed. The same enrichment strategy is employed for the temperature field. Level set functions are used in order to model the crack surface. The accuracy of the method is demonstrated for three examples, one involves the crack propagation due to temperature and mixed traction-temperature loading conditions with complex curved crack paths.

Keywords Fracture · Meshfree · SPH · EFG · MPM

1 Introduction

Meshfree methods have become a powerful alternative to finite element methods. One typical application where meshfree methods still have advantages over finite elements are problems involving fracture. The main advantages of meshfree methods for these problems are their higher-order continuous approximations, ease of adaptive refinement, and the absence of the mesh allowing arbitrary crack growths without re-meshing [5–7,10,20,22,23,34,40,47]. The two former advantages promise high accuracy in comparison to finite element methods, since due to the low-order continuity, the field variables that commonly govern the crack growth are inaccurate around the crack tip.

There are different methods to represent the crack topology in meshfree methods. The first approach was presented by [6], who introduced the so-called visibility criterion. The main idea is to consider the crack as opaque surface and to exclude those nodes from the meshfree approximation which are located on the opposite side of the crack surface. Though the visibility method introduces artificial discontinuities at the crack tip, it remains the most frequently applied method. The diffraction and transparency method [2,3,27] removes the artificial discontinuities of the visibility method but on cost of higher computational effort. These methods are difficult to extend in a three-dimensional setting and often require only approximate calculation of the derivatives of the shape functions. With the development of partition of unity (PU) method [24], meshfree methods were enriched with information of the analytical solution. For example, [13] introduced three opportunities to incorporate the near crack tip solution into the element-free Galerkin (EFG) [6] method:

- Intrinsic PU enrichment
- Extrinsic PU enrichment
- Extrinsic MLS enrichment

S. Wang (✉) · H. Zhang
State Key Laboratory of Subtropical Building Science, South China University of Technology,
Guangzhou 510640, People's Republic of China
E-mail: swangs@hotmail.com

The first two schemes belong to the class of PU enrichments while the last scheme introduces the near crack tip solution directly into the MLS scheme that is the basis of the EFG method. The extrinsic PU enrichment turned out to be particularly efficient since only a few nodes are affected by the enrichment while for the intrinsic PU enrichment, specific (computational cumbersome) techniques are required in order to maintain computational efficiency.

Ventura et al. [47] was the first who took advantage of level set functions [45] for crack representation in the EFG method based on extrinsic PU enrichment. Therefore, the level set function was discretized, and geometric properties such as distance to the crack tip were expressed in terms of discretized level set functions. This implicit representation of the crack is superior to explicit representation of cracks, particularly for complicated crack patterns including curved cracks. Meshfree methods seem superior in this aspect over finite element methods due to their higher-order continuity that avoid kinks which occur at element boundaries in finite element methods. [42] extended the EFG method of [47] to non-linear material behavior, cohesive cracks in dynamics in two- and three-dimensions [37]. They proposed methods with crack front enrichment [42] and without crack front enrichment [49]. In this article, we extend these PU-enriched methods to thermomechanical problems by introducing the temperature as independent field. Thermomechanical fracture analysis is important in many areas e.g. in the automative industry or in aerospace engineering, e.g. to analysis fatigue cracks in engines. We focus our extension to linear elastic fracture mechanics (LEFM) in two-dimensional setting. Therefore, we first summarize briefly the EFG method. Then, we describe the discretization of the displacement and temperature field for two-dimensional crack problems. Afterward, we state the governing equations and derive the weak form. We present some examples that are compared to analytical solutions before we conclude our paper with some remarks and future research perspectives. Our main objective is to provide a more efficient and accurate method for thermomechanical two-dimensional crack problems in linear elastic fracture mechanics.

2 EFG method

The element-free Galerkin method (EFGM) was developed by [6] for applications in computational solid mechanics. EFGM takes advantage of the moving least square (MLS) approximation given by

$$u_i(\mathbf{x}) = \sum_{I \in \mathcal{W}} p_I(\mathbf{x})\, a_I(\mathbf{x}) = \mathbf{p}^T\, \mathbf{a} \tag{1}$$

where $p_I(\mathbf{x})$ denotes polynomial basis functions, $a_I(\mathbf{x})$ are unknown coefficients and $\mathcal{W}$ is the total set of nodes, $u_i(\mathbf{x})$ is the displacement field. In order to guarantee first-order completeness, we use linear functions for $p_I(\mathbf{x})$:

$$p(\mathbf{x}) = [1, x, y] \tag{2}$$

Minimizing a discrete weighted $\mathcal{L}_2$ norm $\mathcal{I}$:

$$\mathcal{I} = \sum_{I \in \mathcal{W}} \left(\mathbf{p}^T(\mathbf{x}_I)\, \mathbf{a}(\mathbf{x}_I) - \mathbf{u}_I\right)^2 w(\mathbf{x} - \mathbf{x}_I, h) \tag{3}$$

with respect to the unknown coefficients leads to the well-known EFG approximation

$$u_i(\mathbf{x}) = \sum_{I \in \mathcal{W}} N_I(\mathbf{x}) u_{iI}(t) = \mathbf{N}^T\, \mathbf{u} \tag{4}$$

with

$$N_I(\mathbf{x}) = \mathbf{p}^T(\mathbf{x})\, A^{-1}(\mathbf{x})\, \mathbf{D}_I(\mathbf{x}) \tag{5}$$

and

$$\begin{aligned} \mathbf{D}_I(\mathbf{x}) &= w(\mathbf{x} - \mathbf{x}_I, h)\mathbf{p}^T(\mathbf{x}_I) \\ \mathbf{A}_I(\mathbf{x}) &= \sum_{I \in \mathcal{W}} w(\mathbf{x} - \mathbf{x}_I, h)\, \mathbf{p}(\mathbf{x}_I)\, \mathbf{p}^T(\mathbf{x}_I) \end{aligned} \tag{6}$$

with the kernel function $w(\mathbf{x}-\mathbf{x}_I, h)$ where h denotes the dilation parameter.

The discretization of the temperature field T, necessary for the thermomechanical formulation described later, is obtained in the same manner yielding the final EFG approximation:

$$T(\mathbf{x}) = \sum_{I \in \mathcal{W}} N_I(\mathbf{x}) T_I(t) \tag{7}$$

with the shape functions $N_I(\mathbf{x})$ given in Eq. (5). Note that in general, different shape functions can be used for the discretization of the thermal and mechanical variables, but we opt to choose the same shape functions for both fields. Nevertheless, we will distinguish them later for clarity by using subscripts M and T for 'mechanical' and 'thermal', respectively.

3 Governing equations and weak form

Consider a domain Ω with temperature boundary Γ_T, flux boundary Γ_q, displacement boundary Γ_u, traction boundary Γ_t, and crack boundary Γ_c such that $\Gamma_T \bigcap \Gamma_q = 0,\ \Gamma = \Gamma_u \bigcup \Gamma_t \bigcup \Gamma_c = \Gamma_T \bigcup \Gamma_q$ and $\Gamma_u \bigcap \Gamma_t = 0,\ \Gamma_c \bigcap \Gamma_t = 0,\ \Gamma_u \bigcap \Gamma_c = 0$. Let us consider adiabatic (traction-free) cracks, i.e. $\Gamma_c \subset \Gamma_q; \bar{q} = 0\ on\ \Gamma_c$, in thermoelasticity under the assumption of small strains. The governing equations are the equilibrium equation and heat equation, respectively, given by

$$\begin{aligned} \sigma_{ij,j} + b_i &= 0_i \qquad \forall \mathbf{x} \in \Omega \\ q_{i,i} + Q &= 0 \qquad \forall \mathbf{x} \in \Omega \end{aligned} \tag{8}$$

where σ_{ij} is the stress tensor, $\mathbf{b}_i$ are the body forces, q_i is the heat flux, and Q denotes the heat source. The compatibility conditions and the constitutive equations in thermoelasticity are given by

$$\begin{aligned} \sigma_{ij} &= C_{ijkl}\epsilon_{kl} \\ \epsilon_{ij} &= \underbrace{\frac{1}{2}\left(u_{i,j} + u_{j,i}\right)}_{\epsilon_{ij}^{mech}} - \underbrace{\alpha_T \Delta T I_{ij}}_{\epsilon_{ij}^{therm}} \\ q_i + kT_{,i} &= 0_i \end{aligned} \tag{9}$$

where C_{ijkl} denotes the first-order elasticity tensor, ϵ_{ij} is the strain tensor where the superscript $mech$ and $therm$ denote the mechanical strain and thermal strain, respectively, α_T is the expansion coefficient, k the diffusivity, ΔT denotes the change in temperature, i.e. $\Delta T = T - T_0$ with room temperature T_0 and I_{ij} is the second-order identity matrix. These equations are complemented by boundary conditions

$$\begin{aligned} u_i &= \bar{u}_i \ \ on\ \ \Gamma_u \\ t_i = \sigma_{ij} n_j &= \bar{t}_i \ \ on\ \ \Gamma_t \\ T &= \bar{T} \ \ on\ \ \Gamma_T \\ q_i n_i &= \bar{q} \ \ on\ \ \Gamma_q \end{aligned} \tag{10}$$

with traction free boundary conditions at the crack surface and where the superimposed bar denotes imposed boundary conditions. The weak form is derived by the method of weighted residuals. Therefore, we multiply the strong form, eq. (8), with a set of admissible test functions $\delta T \in \mathcal{T}_0$ and $\delta u_i \in \mathcal{U}_0$ and integrate over control volume Ω. Integration by parts and using Gauss' divergence theorem leads the final weak form. For adiabatic cracks, we obtain

$$\begin{aligned} \int_\Omega \delta\epsilon_{ij}^{mech}\sigma_{ij}\, d\Omega - \int_\Omega \delta u_i b_i\, d\Omega - \int_{\Gamma_t} \delta u_i \bar{t}_i\, d\Gamma = 0 \\ \int_\Omega \delta q_i k q_i\, d\Omega + \int_\Omega \delta T Q\, d\Omega - \int_{\Gamma_q} \delta T \bar{q}\, d\Gamma = 0 \end{aligned} \tag{11}$$

with the following solution spaces of the test functions δT and δu_i and trial functions $T \in \mathcal{T}$ and $u_i \in \mathcal{U}$

$$\begin{aligned}
\mathcal{U} &= \left\{u_i | u_i \in \mathcal{H}^1,\ u_i = \bar{u}_i \ on\ \Gamma_u,\ u_i\ discontinuous\ on\ \Gamma_c\right\} \\
\mathcal{U}_0 &= \left\{\delta u_i | \delta u_i \in \mathcal{H}^1,\ \delta u_i = 0_i \ on\ \Gamma_u,\ \delta u_i\ discontinuous\ on\ \Gamma_c\right\} \\
\mathcal{T} &= \left\{T | T \in \mathcal{H}^1,\ T = \bar{T}_i \ on\ \Gamma_T,\ T\ discontinuous\ on\ \Gamma_T\right\} \\
\mathcal{T}_0 &= \left\{\delta T | \delta T \in \mathcal{H}^1,\ \delta T = 0 \ on\ \Gamma_T,\ \delta T\ discontinuous\ on\ \Gamma_T\right\}
\end{aligned} \tag{12}$$

where $\mathcal{H}$ denotes the first Hilbert space.

Since the EFG method is not interpolatory, essential boundary conditions cannot be imposed in strong sense as in finite element methods and special techniques are required. Commonly used methods to enforce essential boundary conditions are Lagrange multiplier method [3], coupling to finite element method [9,16,41] or boundary collocation techniques [12]. In this manuscript, we use the boundary collocation technique as described in [15] due to its simplicity and robustness. Details can be found in the given reference. A good overview can be found in [26].

4 Discretization

The basic idea of partition of unity-enriched EFG method is to enrich the test functions and trial functions with information of the analytical solution. Therefore, we decompose the field into a standard part, see Sect. 2, and enriched part:

$$\begin{aligned}
u_i^h(\mathbf{x}) &= u_i^{st}(\mathbf{x}) + u_i^{en}(\mathbf{x}) \\
\delta u_i^h(\mathbf{x}) &= \delta u_i^{st}(\mathbf{x}) + \delta u_i^{en}(\mathbf{x}) \\
T^h(\mathbf{x}) &= T^{st}(\mathbf{x}) + T^{en}(\mathbf{x}) \\
\delta T^h(\mathbf{x}) &= \delta T^{st}(\mathbf{x}) + \delta T^{en}(\mathbf{x})
\end{aligned} \tag{13}$$

The standard part is the EFG approximation as given in Sect. 2 and results in a continuous field away from the crack while the enriched part governs the discontinuous (and singular—at the crack tip) fields:

$$\begin{aligned}
u_i^{enr}(\mathbf{x}) &= \sum_{I \in \mathcal{S}_c} N_I(\mathbf{x})\ S(f(\mathbf{x}_I)) a_{iI} + \sum_{I \in \mathcal{S}_t} N_I(\mathbf{x}) \sum_{K=1}^{4} \mathbf{B}_K b_{iKI} \\
\delta u_i^{enr}(\mathbf{x}) &= \sum_{I \in \mathcal{S}_c} N_I(\mathbf{x})\ S(f(\mathbf{x}_I)) \delta a_{iI} + \sum_{I \in \mathcal{S}_t} N_I(\mathbf{x}) \sum_{K=1}^{4} \mathbf{B}_K \delta b_{iKI} \\
T^{enr}(\mathbf{x}) &= \sum_{I \in \mathcal{S}_c} N_I(\mathbf{x})\ S(f(\mathbf{x}_I)) \tilde{T}_I + \sum_{I \in \mathcal{S}_t} N_I(\mathbf{x}) B \hat{T}_{iI} \\
\delta T^{enr}(\mathbf{x}) &= \sum_{I \in \mathcal{S}_c} N_I(\mathbf{x})\ S(f(\mathbf{x}_I)) \delta \tilde{T}_I + \sum_{I \in \mathcal{S}_t} N_I(\mathbf{x}) B \delta \hat{T}_{iI}
\end{aligned} \tag{14}$$

where a_i, b_i, $\tilde{T}$ and $\hat{T}$ are additional unknowns that needs to be solved for, $\mathcal{S}_c$ are nodes which domain of influence is completely crossed by the crack, Fig. 1, and $\mathcal{S}_t$ are nodes which domain of influence is partially cut by the crack, Fig. 1. All the first terms on the RHS of eq. (14) refer to step function enrichment while all the second terms on the RHS refer to crack tip enrichment. Accordingly, the enrichment functions S, $\mathbf{B}$ and B are choosen; S is the step function that is -1 on one side of the crack and $+1$ on the other side of the crack, Fig. 1, $f(\mathbf{x}_I)$ is the level set function employed to locate the crack:

$$f(\mathbf{x}_I) = \begin{cases} sign\left(\mathbf{n} \cdot [\mathbf{x}_I - \mathbf{x}]\right)\ min\|\mathbf{x} - \mathbf{x}_I\| & \forall \mathbf{x}_I \in \mathcal{S}_c \\ \mathbf{n} \cdot \left(\mathbf{x}_{tip} - \mathbf{x}_I\right) & \forall \mathbf{x}_I \in \mathcal{S}_t \end{cases} \tag{15}$$

where $\mathbf{n}$ is the normal to the crack surface and $\mathbf{x}_{tip}$ is the position of the crack tip.

Equation (14) can also be given in vector and matrix form:

$$\begin{aligned} u_i^h(\mathbf{x}) &= \mathbf{N}_M^u \mathbf{U} + \underbrace{\mathbf{N}_M^a \mathbf{A} + \mathbf{N}_M^b \mathbf{B}}_{u_i^{enr}(\mathbf{x})} \\ \delta u_i^h(\mathbf{x}) &= \mathbf{N}_M^u \delta\mathbf{U} + \underbrace{\mathbf{N}_M^a \delta\mathbf{A} + \mathbf{N}_M^b \delta\mathbf{B}}_{\delta u_i^{enr}(\mathbf{x})} \\ T^h(\mathbf{x}) &= \mathbf{N}_T^u \mathbf{T}_u + \underbrace{\mathbf{N}_T^a \mathbf{T}_a + \mathbf{N}_T^b \mathbf{T}_b}_{T^{enr}(\mathbf{x})} \\ T^h(\mathbf{x}) &= \mathbf{N}_T^u \delta\mathbf{T}_u + \underbrace{\mathbf{N}_T^a \delta\mathbf{T}_a + \mathbf{N}_T^b \delta\mathbf{T}_b}_{\delta T^{enr}(\mathbf{x})} \end{aligned} \tag{16}$$

where we have now also included the 'usual' EFG approximation as described in Sect. 2, i.e. the first term on the RHS; the subscripts and superscripts $M,\ T,\ u,\ a,\ b$ refer to 'mechanical' quantities, 'thermal' quantities, 'usual' degrees of freedom (DOF), step-enriched DOF and tip-enriched DOF, respecitvely. The vectors $\mathbf{U},\ \mathbf{A}$, and $\mathbf{B}$ contain the DOF of the mechanical quantities for the usual part, step-enriched part and tip-enriched part while the vectors $\mathbf{T}_u,\ \mathbf{T}_a$ and $\mathbf{T}_b$ contain the DOF for the thermal quantities. For n nodes with m step-enriched nodes and l tip-enriched nodes, we will have $2n$ ($\mathbf{U}$) plus $2m$ ($\mathbf{A}$) plus $4l$ ($\mathbf{B}$) plus n ($\mathbf{T}_u$) plus m ($\mathbf{T}_a$) plus l ($\mathbf{T}_b$) DOF in the entire discretization. Note that $m, l << n$. The vectors $\mathbf{U},\ \mathbf{A},\ \mathbf{B},\ \mathbf{T}_u,\ \mathbf{T}_a$, and $\mathbf{T}_b$ are stored in one vector $\mathbf{D}$.

For the displacement field, we incorporate the Westergaard solution [48] via the enrichment function

$$\mathbf{B} = \left[\sqrt{r}sin\theta/2,\ \sqrt{r}cos\theta/2,\ \sqrt{r}sin\theta/2\ sin\theta,\ \sqrt{r}cos\theta/2\ sin\theta\right]^T \tag{17}$$

while we use only the first term in order to enrich the temperature field

$$B = \sqrt{r}sin\theta/2 \tag{18}$$

since the heat flux components behave singular like:

$$q_i = \frac{K_{th}}{\sqrt{2\Pi a}} \begin{pmatrix} sin\theta/2 \\ -cos\theta/2 \end{pmatrix} \tag{19}$$

where K_{th} is the thermal intensity factor; r and θ are explained in Fig. 1.

Inserting the test functions and trial functions into the weak form leads to the final fully coupled thermomechanical system of equations that are solved simultaneously with respect to the mechanical *and* thermal degrees of freedom:

$$\mathbf{K}\,\mathbf{D} = \mathbf{F} \tag{20}$$

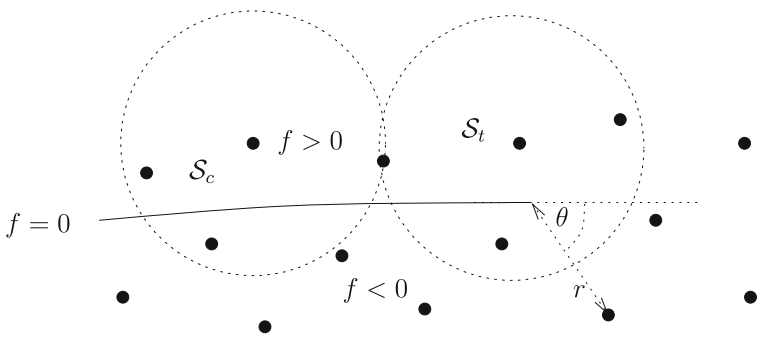

Fig. 1 Modeling crack in meshfree method

with

$$\mathbf{K} = \begin{bmatrix} \mathbf{K}_{MM}^{uu} & \mathbf{K}_{MM}^{ua} & \mathbf{K}_{MM}^{ub} & \mathbf{K}_{MT}^{uu} & \mathbf{K}_{MT}^{ua} & \mathbf{K}_{MT}^{ub} \\ \mathbf{K}_{MM}^{au} & \mathbf{K}_{MM}^{aa} & \mathbf{K}_{MM}^{ab} & \mathbf{K}_{MT}^{au} & \mathbf{K}_{MT}^{aa} & \mathbf{K}_{MT}^{ab} \\ \mathbf{K}_{MM}^{bu} & \mathbf{K}_{MM}^{ba} & \mathbf{K}_{MM}^{bb} & \mathbf{K}_{MT}^{bu} & \mathbf{K}_{MT}^{ba} & \mathbf{K}_{MT}^{bb} \\ \mathbf{K}_{MT}^{uu} & \mathbf{K}_{MT}^{ua} & \mathbf{K}_{MT}^{ub} & \mathbf{K}_{TT}^{uu} & \mathbf{K}_{TT}^{ua} & \mathbf{K}_{TT}^{ub} \\ \mathbf{K}_{MT}^{au} & \mathbf{K}_{MT}^{aa} & \mathbf{K}_{MT}^{ab} & \mathbf{K}_{TT}^{au} & \mathbf{K}_{TT}^{aa} & \mathbf{K}_{TT}^{ab} \\ \mathbf{K}_{MT}^{bu} & \mathbf{K}_{MT}^{ba} & \mathbf{K}_{MT}^{bb} & \mathbf{K}_{TT}^{bu} & \mathbf{K}_{TT}^{ba} & \mathbf{K}_{TT}^{bb} \end{bmatrix} \tag{21}$$

and the vectors $\mathbf{D} = [\mathbf{U}, \mathbf{A}, \mathbf{B}, \mathbf{T}_u, \mathbf{T}_a, \mathbf{T}_b]^T$ and $\mathbf{F} = \left[\mathbf{F}_M^u, \mathbf{F}_M^a, \mathbf{F}_M^b, \mathbf{F}_T^u, \mathbf{F}_T^a, \mathbf{F}_T^b\right]^T$ where $\mathbf{U}$, $\mathbf{A}$ and $\mathbf{B}$ are the vectors contains the displacement degrees of freedom $\mathbf{u}$, $\mathbf{a}$ and $\mathbf{b}$, respectively, where the indices M and T refer to mechanical and thermal quantities, the indices u, a and b to the degrees of freedom and $\mathbf{N}$ and $\mathbf{B}$ contain the shape functions and their derivatives; $\mathbf{C}$ is the first-order elasticity tensor and the tensor $\mathbf{D}$ contains the diffusity k. Note that we use the same shape functions for the mechanical and temperature fields, i.e. $\mathbf{N}_T = \mathbf{N}_M$; see also for example Eq. (14). The force vectors $\mathbf{F}_M^i$, $i = u, a, b$ refer to mechanical loading, see the last two terms on the LHS in the first line of Eq. (8) while the force vectors $\mathbf{F}_T^i$, $i = u, a, b$ refer to thermal loading, the last two terms on the LHS in the second line of Eq. (8). These vectors are stored in the vector $\mathbf{F}$. The submatrices of $\mathbf{K}$ and $\mathbf{F}$ are given for sake of completeness in the appendix, Sect. 7.

5 Examples

We present three examples. The first two examples are verification of the method by comparing results of our method to other analytical results. The last problems show the ability of our method to handle crack propagation problems. The main advantage of the proposed method is that it can handle crack growth with ease.

5.1 Rectangular plate with a center crack

Consider a rectangular plate with a center crack. The dimensions are illustrated in Fig. 2a and we have chosen $L = W$. Only thermal boundary conditions are applied as illustrated in the figure with $\bar{T} = 10^o$ Celsius. This problem was solved previously by [25,28]. Results are shown for different ratios a/W. [28] used a computationally expensive boundary element method to solve this problem while handbook solutions are given in [25]. In this study, we adopt the presentation of the results from [25,28] and give the results in the table form.

We tested unstructured particle arrangements and different refinements and present results starting from approximately 500 nodes up to 4,000 nodes. For finer discretizations of 2,000 nodes and above, the spacing between the particles is similar (almost equi-spaced) in the unstructured discretization as illustrated in

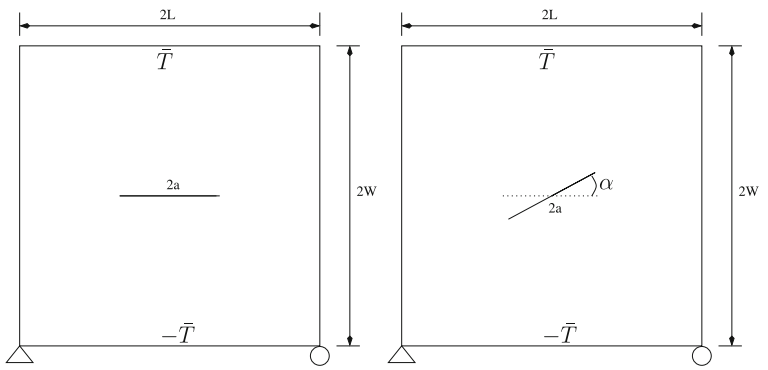

(a) Plate with centre crack **(b)** Plate with slant crack

Fig. 2 Rectangular plate with crack

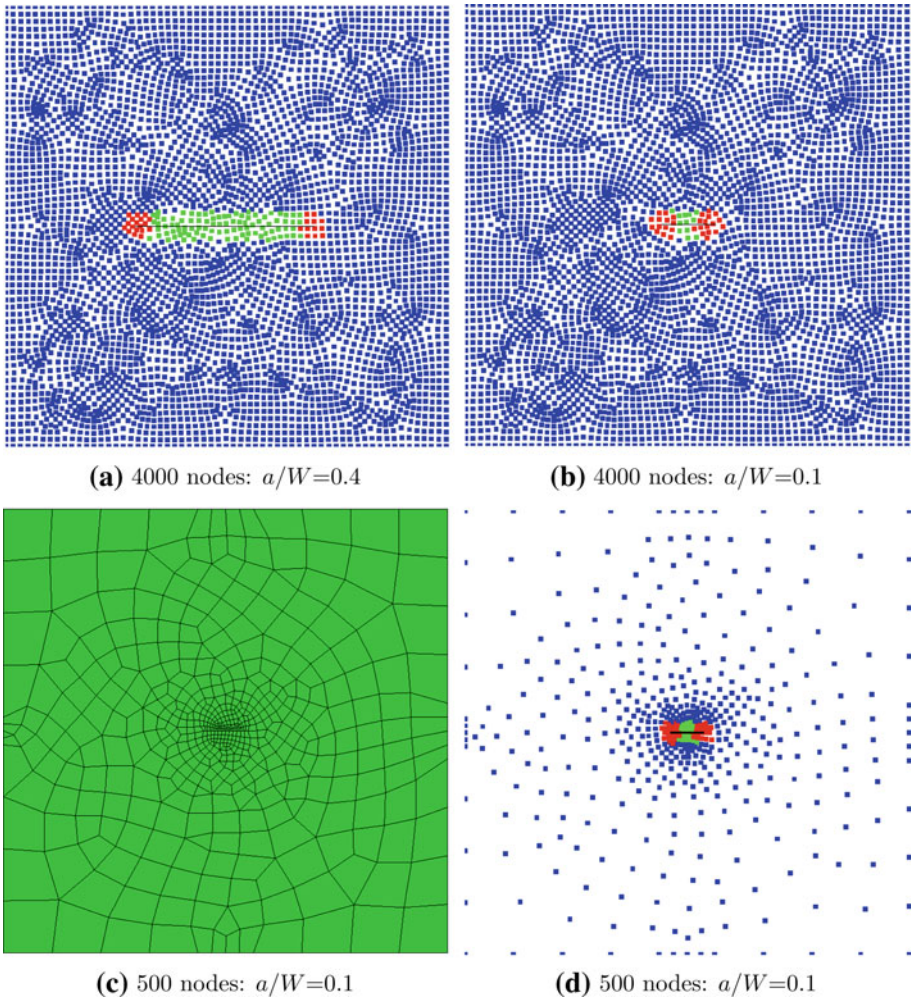

Fig. 3 Discretization of the plate with a crack problem for different discretizations and different crack lengths

Fig. 3a,b for different crack lengths. The size of the domain of influence is coupled to the nodal spacing and is approximately 1.8 times the average nodal spacing $d = \sqrt{dx^2 + dy^2}$ where dx and dy are the distances between neighboring nodes in x and y direction. The step-enriched degrees of freedom are illustrated in green color while tip-enriched degrees of freedom are shown in red color. A small domain of influence is chosen according to [30,32] though the accuracy can be improved by increasing the support size, see e.g. [36]. It is also noted that structured arrangements lead to an improved accuracy in meshfree methods [31,33], but we have used unstructured arrangements since they are commonly used for modeling complex geometries. Note that for the very coarse discretization of only 500 nodes, equi-spaced node arrangements were only achieved for $a/W > 0.4$. Otherwise, the nodal density is higher in the vicinity of the crack as illustrated for approximately 500 nodes and an $a/W = 0.1$ in Fig. 3c,d. A refinement around the crack tip is needed since crack tip enrichments influencing each other will result in deterioration of accuracy as noted e.g. by [37,43]. As can be seen in Fig. 3c,d, the two tip-enriched nodes do not influence each other in the given discretization. Tip-enriched nodes are illustrated again in green color while step-enriched nodes are shown in red. The procedure of computing the size of the domain of influence is described in detail in the meshfree literature, e.g. the excellent books of [1,21].

The results are summarized in Table 1 in accordance with the published results by [25,28]. They agree well with these results. Moreover, even for only 500 nodes, we were able to obtain results independent of the refinement. Note the key advantage of our method is that crack propagation can be modeled with ease since no re-meshing is needed; a crack propagation problem will be shown in the last example. Another advantage of our method is the increased accuracy obtained through including information of the analytical solution into

Table 1 Comparison of the stress intensity factor K_{II} of our method for three different refinements (500 nodes–4,000 nodes) compared to the results in [25,28]

a/W	500 Nodes	2,000 Nodes	4, 000 Nodes	[28]	[25]
0.1	0.019	0.020	0.020	0.018	0.021
0.2	0.053	0.054	0.054	0.054	0.053
0.3	0.094	0.095	0.095	0.095	0.094
0.4	0.141	0.141	0.141	0.141	0.141
0.5	0.188	0.189	0.189	0.190	0.188
0.6	0.244	0.245	0.245	0.243	0.247

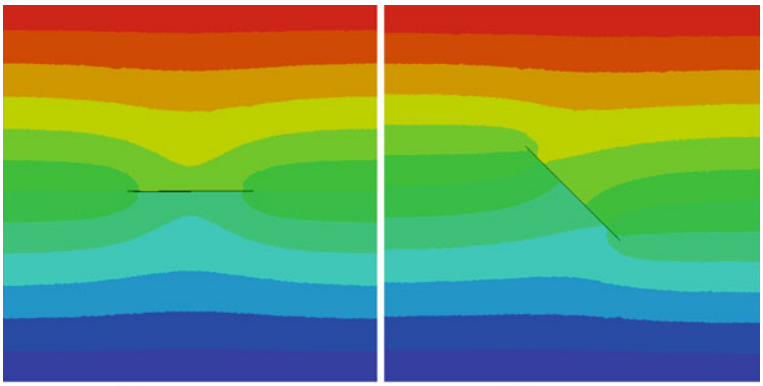

(a) Centre crack **(b)** Slant crack

Fig. 4 Temperature field for problem: rectangular plate with crack

the approximation. Even with extremely coarse meshes, high accuracy is achieved. We do not give a detailed comparison since in our opinion, it is difficult to compare the accuracy over the computation time since the efficiency is greatly affected by the implementation. The temperature field is illustrated in Fig. 4a.

5.2 Rectangular plate with a slant crack

In this example, the dimensions of the problem remain the same as for the previous problem, but the crack is now inclined against the global x-axis resulting in mixed-mode fracture. We used the same particle arrangements and show the stress intensity factors K_I and K_{II} for different ratios a/W exemplary for discretization with 2,000 nodes. The results of the coarser and finer discretizations are very similar. The summary of results is shown in Table 2 and 3, and the agreement with results from other authors is very close. The temperature field for one inclination is shown in Fig. 4b.

5.3 Crack growth in rectangular plate

Finally, we study a crack propagation problem. Therefore, consider the rectangular plate with a central crack of length a (Fig. 5). Experimental results [29] of this problem are available for different loads. The load conditions

Table 2 Comparison of the stress intensity factor K_I and K_{II} of our method compared to the results in [25,28] for $a/W = 0.3$ and varying α

α	Our method K_I	K_I [28]	K_I [25]	Our method K_{II}	K_{II} [28]	K_{II} [25]
0°	0.000	0.000	0.000	0.054	0.054	0.054
15°	0.0036	0.0036	0.0038	0.054	0.054	0.054
30°	0.0066	0.0064	0.0071	0.048	0.048	0.048
45°	0.0073	0.0071	0.0077	0.041	0.041	0.042
60°	0.0050	0.0049	0.0053	0.032	0.032	0.032
75°	0.0014	0.0010	0.0023	0.018	0.018	0.018
90°	0.0001	0.0003	0.000	0.000	0.000	0.000

are summarized in Table 4. The main feature of these experiments with different boundary conditions are as follows: while the crack propagates almost perpendicular to the load direction when a traction load is applied (case 2–4), the crack propagation upwards and turns toward the right-hand side when only temperature load is applied at the upper and lower boundary.

We tested all cases but present only result of case (1) and (3) since they present the key features of the crack path. We used discretizations from 850 up to 4,000 nodes and show results for 4,000 nodes since the results even for 850 nodes look almost identical to the results obtained with the fine discretization. The direction of the crack is determined by the maximum hoop stress criterion, see e.g. [46,50]. The crack length is controlled in all our simulations and set to 0.5 a; a illustrated in Fig. 5. Details on the level set update are given elsewhere [42,47].

In Fig. 6, one can see the temperature field and the almost straight crack path for case (3) when a traction load is applied at the top boundary in addition to temperature boundary conditions. The von Mises-stresses and

Table 3 Comparison of the stress intensity factor K_I and K_{II} of our method compared to the results in [25,28] for $\alpha = 30^o$ and varying a/W

a/W	Our method K_{II}	K_{II} [28]	K_{II} [25]	Our method K_I	K_I [28]	K_I [25]
0.2	0.030	0.030	0.030	0.002	0.002	0.002
0.3	0.048	0.048	0.048	0.007	0.006	0.008
0.4	0.065	0.064	0.064	0.014	0.014	0.015
0.5	0.076	0.076	0.076	0.026	0.026	0.027
0.6	0.087	0.087	0.086	0.040	0.040	0.041

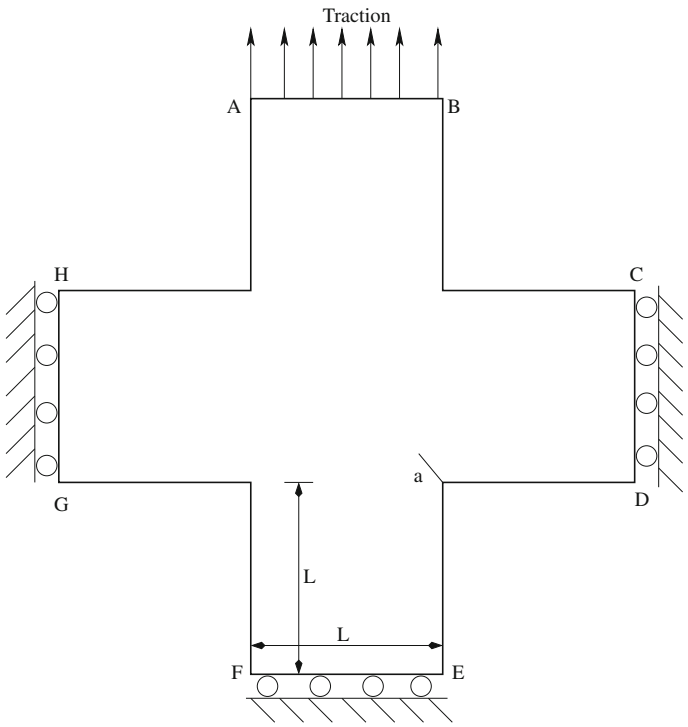

Fig. 5 Rectangular plate with a central crack

Table 4 Load conditions for the problem shown in Fig. 5 as presented by [29]

Load	Temperature [°C]		Traction [Pa]
	AB	EF	AB
Case (1)	10	−10	0
Case (2)	0	0	10
Case (3)	10	−10	10

(a) Case (1) **(b)** Case (3)

Fig. 6 Crack path and temperature field for different load cases for problem shown in Fig. 5

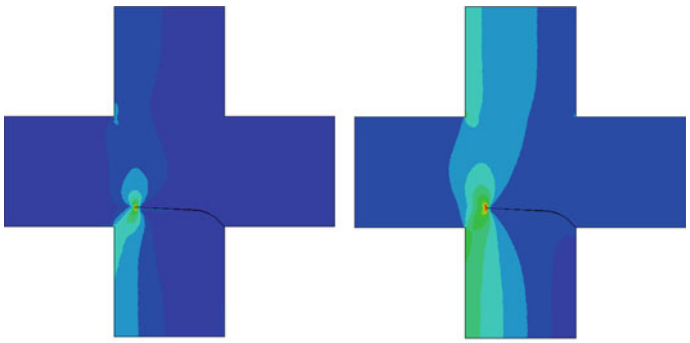

(a) von Mises stress **(b)** σ_y

Fig. 7 Stress distribution for case (3) for the problem in Fig. 5

the normal stress in load direction σ_y are illustrated in Fig. 7. Figure 6a shows the results for case (1) where only temperature is applied. The key features, i.e. the correct crack pattern is captured by our simulation very nicely.

6 Conclusion and research perspectives

We have presented an enriched meshfree method for thermoelastic two-dimensional crack problems. Therefore, enrichment functions are introduced in the discretization that accurately represent features of the analytical solution; we note that the analytical solution does not need to be known exactly. It is sufficient to know basic features of the analytical solution. The thermal as well as the displacement field is locally, i.e. in the vicinity of the crack, enhanced with enrichment functions that capture the discontinuity in the thermal and displacement field as well as the singularity in both fields at the crack tip. The *local* character of the enrichment guarantees an optimum between accuracy and efficiency of the method.

The crack is represented by level set functions that are discretized with the same meshfree shape functions as for the thermal and displacement variables. Therefore, the existing discretization can be exploited in order to describe the topology of the crack without explicit representation. The key feature of the method is its ability to handle complex and curved crack path with ease. The crack can propagate arbitrarily through a given discretization. The higher-order continuity of the meshfree method has clear advantages over a discretization with finite elements since the smoothness and higher-order continuity guarantees the propagation of curved cracks even for very coarse discretizations.

We applied the method to three problems where analytical and experimental data are available. The first two numerical examples dealt with problems without crack propagation. We showed that even with a very coarse discretization, we were able to achieve high accuracy. This is attributed mainly to the enrichment strategy. We have also shown that complicated and curved crack paths can be obtained with our method that agrees

well with published data from experiments [29]. That was shown for pure temperature loading and mixed traction/temperature loading.

In the future, this concept can be extended to other interesting phenomena such as shear bands where temperature effects govern the motion of the shear band [18,19,38,39,44]. The method is particularly attractive for extensions to 3D since crack propagation in meshfree methods can be easier implemented as compared in finite element and extended finite element methods [4,8,11,14,17,35,37,43].

7 Appendix: submatrices

$$
\begin{aligned}
\mathbf{K}_{MM}^{uu} &= \int_{\Omega} \mathbf{B}_{Mu}\mathbf{C}\mathbf{B}_{Mu}^{T}\, d\Omega, \quad \mathbf{K}_{MM}^{ua} = \int_{\Omega} \mathbf{B}_{Mu}\mathbf{C}\mathbf{B}_{Ma}^{T}\, d\Omega \\
\mathbf{K}_{MM}^{ub} &= \int_{\Omega} \mathbf{B}_{Mu}\mathbf{C}\mathbf{B}_{Mb}^{T}\, d\Omega, \quad \mathbf{K}_{MM}^{aa} = \int_{\Omega} \mathbf{B}_{Ma}\mathbf{C}\mathbf{B}_{Ma}^{T}\, d\Omega \\
\mathbf{K}_{MM}^{ab} &= \int_{\Omega} \mathbf{B}_{Ma}\mathbf{C}\mathbf{B}_{Mb}^{T}\, d\Omega, \quad \mathbf{K}_{MM}^{bb} = \int_{\Omega} \mathbf{B}_{Mb}\mathbf{C}\mathbf{B}_{Mb}^{T}\, d\Omega \\
\mathbf{K}_{MT}^{uu} &= \int_{\Omega} \mathbf{B}_{Mu}\mathbf{C}\alpha_{T}\mathbf{N}_{Tu}^{T}\, d\Omega, \quad \mathbf{K}_{MT}^{ua} = \int_{\Omega} \mathbf{B}_{Mu}\mathbf{C}\alpha_{T}\mathbf{N}_{Ta}^{T}\, d\Omega \\
\mathbf{K}_{MT}^{ub} &= \int_{\Omega} \mathbf{B}_{Mu}\mathbf{C}\alpha_{T}\mathbf{N}_{Tb}^{T}\, d\Omega, \quad \mathbf{K}_{MT}^{au} = \int_{\Omega} \mathbf{B}_{Ma}\mathbf{C}\alpha_{T}\mathbf{N}_{Tu}^{T}\, d\Omega \\
\mathbf{K}_{MT}^{aa} &= \int_{\Omega} \mathbf{B}_{Ma}\mathbf{C}\alpha_{T}\mathbf{N}_{Ta}^{T}\, d\Omega, \quad \mathbf{K}_{MT}^{ab} = \int_{\Omega} \mathbf{B}_{Ma}\mathbf{C}\alpha_{T}\mathbf{N}_{Tb}^{T}\, d\Omega \\
\mathbf{K}_{MT}^{bu} &= \int_{\Omega} \mathbf{B}_{Mb}\mathbf{C}\alpha_{T}\mathbf{N}_{Tu}^{T}\, d\Omega, \quad \mathbf{K}_{MT}^{ba} = \int_{\Omega} \mathbf{B}_{Mb}\mathbf{C}\alpha_{T}\mathbf{N}_{Ta}^{T}\, d\Omega \\
\mathbf{K}_{MT}^{bb} &= \int_{\Omega} \mathbf{B}_{Mb}\mathbf{C}\alpha_{T}\mathbf{N}_{Tb}^{T}\, d\Omega, \quad \mathbf{K}_{TT}^{uu} = \int_{\Omega} \mathbf{B}_{Tu}\mathbf{D}\mathbf{B}_{Tu}^{T}\, d\Omega \\
\mathbf{K}_{TT}^{ua} &= \int_{\Omega} \mathbf{B}_{Tu}\mathbf{D}\mathbf{B}_{Ta}^{T}\, d\Omega, \quad \mathbf{K}_{TT}^{ub} = \int_{\Omega} \mathbf{B}_{Tu}\mathbf{D}\mathbf{B}_{Tb}^{T}\, d\Omega \\
\mathbf{K}_{TT}^{aa} &= \int_{\Omega} \mathbf{B}_{Ta}\mathbf{D}\mathbf{B}_{Ta}^{T}\, d\Omega, \quad \mathbf{K}_{TT}^{ab} = \int_{\Omega} \mathbf{B}_{Ta}\mathbf{D}\mathbf{B}_{Tb}^{T}\, d\Omega \\
\mathbf{K}_{TT}^{bb} &= \int_{\Omega} \mathbf{B}_{Tb}\mathbf{D}\mathbf{B}_{Tb}^{T}\, d\Omega
\end{aligned}
\tag{22}
$$

$$
\begin{aligned}
\mathbf{F}_{M}^{u} &= \int_{\Omega} \mathbf{N}_{Mu}\mathbf{b}\, d\Omega + \int_{\Gamma_t} \mathbf{N}_{Mu}\bar{\mathbf{t}}\, d\Gamma \\
\mathbf{F}_{M}^{a} &= \int_{\Omega} \mathbf{N}_{Ma}\mathbf{b}\, d\Omega + \int_{\Gamma_t} \mathbf{N}_{Ma}\bar{\mathbf{t}}\, d\Gamma, \quad \mathbf{F}_{M}^{b} = \int_{\Omega} \mathbf{N}_{Mb}\mathbf{b}\, d\Omega + \int_{\Gamma_t} \mathbf{N}_{Mb}\bar{\mathbf{t}}\, d\Gamma \\
\mathbf{F}_{T}^{u} &= \int_{\Omega} \mathbf{N}_{Tu}\mathbf{Q}\, d\Omega + \int_{\Gamma_q} \mathbf{N}_{Tu}\bar{\mathbf{q}}\, d\Gamma, \quad \mathbf{F}_{T}^{a} = \int_{\Omega} \mathbf{N}_{Ta}\mathbf{Q}\, d\Omega + \int_{\Gamma_q} \mathbf{N}_{Ta}\bar{\mathbf{q}}\, d\Gamma \\
\mathbf{F}_{T}^{b} &= \int_{\Omega} \mathbf{N}_{Tb}\mathbf{Q}\, d\Omega + \int_{\Gamma_q} \mathbf{N}_{Tb}\bar{\mathbf{q}}\, d\Gamma
\end{aligned}
\tag{23}
$$

References

1. Atluri, S.: The Meshless Local Petrov-Galerkin (MLPG) Method. Tech Science Press, Los Angeles (2002)
2. Belytschko, T., Fleming, M.: Smoothing, enrichment and contact in the element free galerkin method. Comput. Struct. **71**, 173–195 (1999)
3. Belytschko, T., Krongauz, Y., Organ, D., Fleming, M., Krysl, P.: Meshless methods: an overview and recent developments. Comput. Methods Appl. Mech. Eng. **139**, 3–47 (1996)
4. Belytschko, T., Krysl, P., Krongauz, Y.: A three-dimensional explicit element-free galerkin method. Int. J. Numer. Methods Fluids **24**, 1253–1270 (1997)
5. Belytschko, T., Lu, Y.: Element-free galerkin methods for static and dynamic fracture. Int. J. Solids Struct. **32**, 2547–2570 (1995)
6. Belytschko, T., Lu, Y., Gu, L.: Element-free galerkin methods. Int. J. Numer. Methods Fluids **37**, 229–256 (1994)
7. Belytschko, T., Lu, Y., Gu, L.: Crack propagation by element-free galerkin methods. Eng. Fract. Mech. **51**(2), 295–315 (1995)
8. Belytschko, T., Moran, N.S.B., Black, T.: An element-free galerkin method for three-dimensional fracture mechanics. Comput. Mech. **20**(1), 70–175 (1997)
9. Belytschko, T., Organ, D., Krongauz, Y.: A coupled finite element-element-free Galerkin method. Comput. Mech. **17**, 186–195 (1995)
10. Belytschko, T., Tabbara, M.: Dynamic fracture using element-free galerkin methods. Int. J. Numer. Methods Eng. **39**(6), 923–938 (1996)
11. Bordas, S., Rabczuk, T., Zi, G.: Three-dimensional crack initiation, propagation, branching and junction in non-linear materials by extrinsic discontinuous enrichment of meshfree methods without asymptotic enrichment. Eng. Fract. Mech. **75**, 943–960 (2008)
12. Chen, J., Wang, H.: New boundary condition treatments in meshfree computation of contact problems. Comput. Methods Appl. Mech. Eng. **187**, 441–468 (2000)
13. Fleming, M., Chu, Y., Moran, B., Belytschko, T.: Enriched element-free galerkin methods for crack tip fields. Int. J. Numer. Methods. Eng. **40**, 1483–1504 (1997)
14. Gato, C., Shie, Y.: Detonation-driven fracture in thin shell structures: numerical studies. Comb. Explos. Shock Wave. **46**(1), 103–110 (2010)
15. Gunther, F., Liu, W.: Implementation of boundary conditions for meshless methods. Comput. Methods Appl. Mech. Eng. **163**, 205–230 (1998)
16. Krongauz, Y., Belytschko, T.: Enforcement of essential boundary conditions in meshless approximations using finite elements. Comput. Methods Appl. Mech. Eng. **131**, 133–145 (1996)
17. Krysl, P., Belytschko, T.: The element free galerkin method for dynamic propagation of arbitrary 3-d cracks. Int. J. Numer. Methods. Eng. **44**(6), 767–800 (1999)
18. Li, S., Hao, W., Liu, W.: Mesh-free simulations of shear banding in large deformation. Int. J. Solids Struct. **37**, 7185–7206 (2000)
19. Li, S., Liu, W., Rosakis, A., Belytschko, T., Hao, W.: Mesh free galerkin simulations of dynamic shear band propagation and failure mode transition. Int. J. Solids Struct. **39**, 1213–1240 (2002)
20. Li, S., Simonson, B.C.: Meshfree simulation of ductile crack propagation. Int. J. Comput. Methods Eng. Sci. Mech. **6**, 1–19 (2003)
21. Liu, G.: Smooth Particle Hydrodynamics: A Meshfree Particle Method (2003)
22. Liu, K., Long, S., Li, G.: A meshless local petrov-galerkin method for the analysis of cracks in the isotropic functionally graded material. Comput. Mater. Contin. **7**, 43–57 (2008)
23. Liu, W., Jun, S., Zhang, Y.: Reproducing kernel particle methods. Int. J. Numer. Methods Eng. **20**, 1081–1106 (1995)
24. Melenk, J.M., Babuska, I.: The partition of unity finite element method: basic theory and applications. Comput. Methods Appl. Mech. Eng. **139**, 289–314 (1996)
25. Murakami, Y.: Stress Intensity Factors Handbook. Pergamon Press, Oxford (1987)
26. Nguyen, V., Rabczuk, T., Bordas, S., Duflot, M.: Meshless methods: a review and computer implementation aspects. Math. Comput. Simul. **79**, 763–813 (2008)
27. Organ, D., Fleming, M., Terry, T., Belytschko, T.: Continuous meshless approximations for nonconvex bodies by diffraction and transparency. Comput. Mech. **18**, 225–235 (1996)
28. Prasad, N., Aliabadi, M., Rooke, D.: The dual boundary element method for thermoelstic crack growth. Int. J. Fract. **66**, 252–272 (1994)
29. Prasad, N., Aliabadi, M., Rooke, D.: Incremental crack growth in thermoelastic problems. Int. J. Fract. **66**, R45–R50 (1994)
30. Rabczuk, T., Areias, P.: A meshfree thin shell for arbitrary evolving cracks based on an extrinsic basis. Comput. Model. Eng. Sci. **16**(2), 115–130 (2006)
31. Rabczuk, T., Areias, P., Belytschko, T.: A meshfree thin shell method for non-linear dynamic fracture. Int. J. Numer. Methods Eng. **72**(5), 524–548 (2007)
32. Rabczuk, T., Belytschko, T.: Cracking particles: A simplified meshfree method for arbitrary evolving cracks. Int. J. Numer. Methods Eng. **61**(13), 2316–2343 (2004)
33. Rabczuk, T., Belytschko, T.: Adaptivity for structured meshfree particle methods in 2d and 3d. Int. J. Numer. Methods Eng. **63**(11), 1559–1582 (2005)
34. Rabczuk, T., Belytschko, T.: Application of particle methods to static fracture of reinforced concrete structures. Int. J. Fract. **137**(1–4), 19–49 (2006)
35. Rabczuk, T., Belytschko, T.: A three dimensional large deformation meshfree method for arbitrary evolving cracks. Comput. Methods Appl. Mech. Eng. **196**, 2777–2799 (2007)
36. Rabczuk, T., Belytschko, T., Xiao, S.: Stable particle methods based on lagrangian kernels. Comput. Methods Appl. Mech. Eng. **193**(12–14), 1035–1063 (2004)

37. Rabczuk, T., Bordas, S., Zi, G.: A three-dimensional meshfree method for continuous multiple crack initiation, nucleation and propagation in statics and dynamics. Comput. Mech. **40**(3), 473–495 (2007)
38. Rabczuk, T., Areias, P.M.A., Belytschko, T.: A simplified mesh-free method for shear bands with cohesive surfaces. Int. J. Numer. Methods Eng. **69**(5), 993–1021 (2007)
39. Rabczuk, T., Samaniego, E.: Discontinuous modelling of shear bands using adaptive meshfree methods. Comput. Methods Appl. Mech. Eng. **197**, 641–658 (2008)
40. Rabczuk, T., Song, J.-H., Belytschko, T.: Simulations of instability in dynamic fracture by the cracking particles method. Eng. Fract. Mech. **76**, 730–741 (2009)
41. Rabczuk, T., Xiao, S., Sauer, A.: Coupling of mesh-free methods with finite elements: basic concepts and test results. Commun. Numer. Methods Eng. **22**(10), 1031–1065 (2006)
42. Rabczuk, T., Zi, G.: A meshfree method based on the local partition of unity for cohesive cracks. Comput. Mech. **39**(6), 743–760 (2007)
43. Rabczuk, T., Zi, G., Bordas, S., Nguyen-Xuan, H.: A geometrically non-linear three dimensional cohesive crack method for reinforced concrete structures. Eng. Fract. Mech. **75**, 4740–4758 (2008)
44. Hao, W.K., Liu, S., Quian, D.: Localization-induced band and cohesive model. J. Appl. Mech.-Trans. ASME **67**(4), 803–812 (2000)
45. Sethian, I.: Level set methods and fast marching methods: evolving interfaces in computational geometry, fluid mechanics, computer vision and materials science. Cambridge University Press, Cambridge (1999)
46. Soh, A., Liu, J., Lee, K.: On a moving griffith crack in anisotropic piezoelectric solids. Arch. Appl. Mech. **72**(6–7), 458–469 (2002)
47. Ventura, G., Xu, J., Belytschko, T.: A vector level set method and new discontinuity approximation for crack growth by EFG. Int. J. Numer. Methods Eng. **54**(6), 923–944 (2002)
48. Westergaard, H.: J. Appl. Mech. **6**(A), 49–53 (1937)
49. Zi, G., Rabczuk, T., Wall, W.: Extended meshfree methods without branch enrichment for cohesive cracks. Comput. Mech. **40**(2), 367–382 (2007)
50. Zybell, L., Muhlich, U., Kuna, M.: Constitutive equations for porous plane-strain gradient elasticity obtained by homogenization. Arch. Appl. Mech. **79**(4), 359–375 (2009)